An Effective Induction Motor Control for Photovoltaic Pumping

Montiê Alves Vitorino, Maurício Beltrão de Rossiter Corrêa, *Member, IEEE*,
Cursino Brandão Jacobina, *Senior Member, IEEE*, and Antonio Marcus Nogueira Lima, *Senior Member, IEEE*

***Abstract*—A new design of an efficient batteryless pumping system powered from photovoltaic panels, comprising a push–pull converter and an induction motor, is presented. Detailed evaluation of the energy processing cycle has allowed the formulation of a set of design principles and the optimization of a sensorless induction motor drive system. The resulting performance enhancement is demonstrated experimentally.**

***Index Terms*—Induction motor, photovoltaic, pumping, sensorless.**

I. Introduction

PHOTOVOLTAIC technology is one of the most promising for distributed low-power electrical generation. The steady reduction of price per peak watt over recent years and the simplicity with which the installed power can be increased by adding panels are some of its attractive features. Among the many applications of photovoltaic energy, pumping is one of the most promising. In a photovoltaic pump-storage system, solar energy is stored, when sunlight is available, as potential energy in a water reservoir and consumed according to demand. There are advantages in avoiding the use of large banks of lead-acid batteries, which are heavy and expensive and have one-fifth of the lifetime of a photovoltaic panel. It is important, however, that the absence of batteries does not compromise the efficiency of the end-to-end power conversion chain, from panels to mechanical pump.

A typical configuration of a batteryless photovoltaic pumping system is shown in Fig. 1. The system comprises the following components: 1) photovoltaic panels; 2) dc/dc converter; 3) dc/ac inverter; 4) induction motor; and 5) centrifugal pump. The design of an effective photovoltaic pumping system without the use of a battery bank represents a significant challenge. It is necessary to deal with the effect of the stochastic nature of solar insolation on the entire energy conversion chain, including the nonlinear characteristics of photovoltaic panels, the voltage boost converter, and the electromechanical power conversion device. In general terms, it is necessary to obtain the best performance from each system component over a wide input power range.

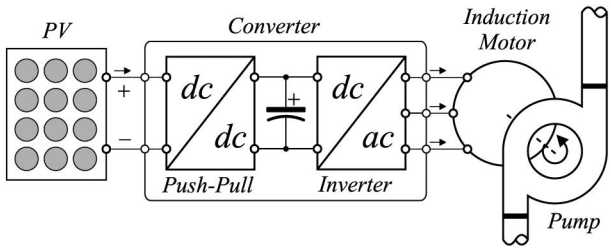

Fig. 1. Basic components of a photovoltaic pumping system not requiring a lead-acid battery bank.

Photovoltaic panels require specific control techniques to ensure operation at their maximum power point (MPP). Impedance matching issues mean that photovoltaic arrays may operate more or less efficiently, depending on their series/parallel configuration [1], [2]. In this paper, a minimum number of series connections are adopted. This means that a relatively high dc voltage gain (between six and ten) is necessary to provide the drive voltage required by the induction motor. The proposed system uses a push–pull converter and is based on the solution presented in [3]. The choice for this specific dc/dc converter topology is basically dictated by the requirement for galvanic isolation between the low- and high-voltage sides. Such a requirement precludes the use of low-cost and high-efficiency converter topologies [4]–[6]. A study of how the converter topology affects the MPP tracking (MPPT) of a photovoltaic system is reported in [7] and [8].

In addition to its voltage-boosting function, required for load matching, the dc/dc converter implements MPPT for the photovoltaic array. Several MPPT methods have been described in the technical literature [2], [9]–[20]. Some consider specific conditions, such as partial shadowing [21]–[23] or fast insolation change [24]. For the sake of simplicity, the MPPT used in this paper is based on the incremental conductance algorithm [18].

Electromechanical power conversion is provided by a delta-connected three-phase induction motor fed by a standard insulated-gate bipolar-transistor voltage-source inverter. Connecting the motor windings in delta reduces the voltage gain requirement. Assuming that the panels generate a time-varying MPPT, it is necessary to ensure electromechanical power conversion with minimum loss at all operating points. Highly efficient induction motor drive systems can be realized using

Manuscript received July 31, 2009; revised December 23, 2009 and April 20, 2010; accepted May 27, 2010. Date of publication June 28, 2010; date of current version March 11, 2011. This work was supported in part by the National Council for Scientific and Technological Development (CNPq), by the Coordination of Improvement of Higher Education Personnel (CAPES), and by the Foundation for Research Support of the State of Paraíba (FAPESQ).

The authors are with the Department of Electrical Engineering, Federal University of Campina Grande, Campina Grande 58429-900, Brazil (e-mail: vitorino@ee.ufcg.edu.br; mbrcorrea@dee.ufcg.edu.br; jacobina@dee.ufcg.edu.br; amnlima@dee.ufcg.edu.br).

Digital Object Identifier 10.1109/TIE.2010.2054053

0278-0046/$26.00 © 2010 IEEE

field-oriented control strategies. However, these strategies require rotor speed measurement, which is a drawback in terms of cost and reliability. Several induction-motor-based solutions have been proposed for photovoltaic pumping [25]–[32]. In [25], the photovoltaic panels are connected in parallel with the dc-link capacitor bank, and a two-level inverter operates in a six-step mode, with the MPPT being determined by the motor slip frequency. This is a low-cost solution but requires series connection of several panels and is therefore highly susceptible to impedance matching problems. A solution based on slip frequency adjustment is described in [26], but this is less than optimum in terms of motor efficiency. In [27]–[31], vector control is exploited, but motor efficiency was not considered as a design requirement. Solutions based on speed measurement generally decrease reliability and increase cost. Solutions based on speed estimation, such as the one presented in [32], can be adopted, but in this case, motor parameter dependence is an important issue. It is important to note that vector control strategies are not, in themselves, sufficient to maximize motor efficiency, and consequently, an optimization algorithm must be added to the control loop. This has been recorded in [33]–[36], where constant speed and a stiff dc-bus voltage are adopted. Neither condition applies to the system configuration studied here. Nevertheless, it is possible to adapt such solutions for the case where input power does not depend on load demand but on the availability of sunlight. Sensorless solutions [37]–[39], along with optimization of motor efficiency, are proposed here to maximize the potential energy of the water pumped, given the available solar energy. Since batteries are not used, motor operation will generally be below rated power. Maximization of efficiency is nevertheless maintained.

Control and design improvements to achieve an effective photovoltaic pumping system are addressed in this paper. The end-to-end power chain from the photovoltaic panel to the motor shaft is evaluated. In Section II, the basic principle of push–pull operation is discussed. Section III presents the control strategies and optimization principles. In Section IV, the control and optimization procedures are evaluated. Section V contains our concluding remarks.

II. Voltage Boost

The dc/dc converter boosts the photovoltaic panel voltage up to the value required to drive an off-the-shelf induction motor. This is needed to accommodate the requirement that relatively few photovoltaic panels be connected in series. The push–pull converter topology ensures galvanic isolation between input and output voltages, as well as provides the required voltage gain. The basic circuit diagram of the step-up converter is shown in Fig. 2. The operation of this converter relies on the time intervals in which power switches q_a and q_b conduct. Fig. 3 shows a typical switching pattern for one period T. In this figure, D denotes the duty cycle defined by

$$D = \frac{t_{\text{on}}}{T} \tag{1}$$

where t_{on} corresponds to the total time interval that both switches conduct ($t_{\text{on}} = DT$). The output voltage (E) depends on the input voltage (V), the duty cycle (D), and the high-frequency transformer turns ratio (n), i.e.,

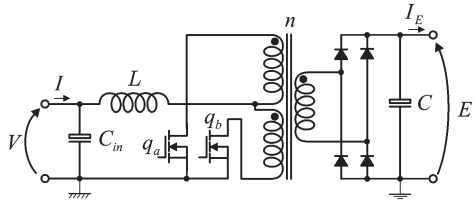

Fig. 2. Basic circuit diagram of the step-up dc/dc converter.

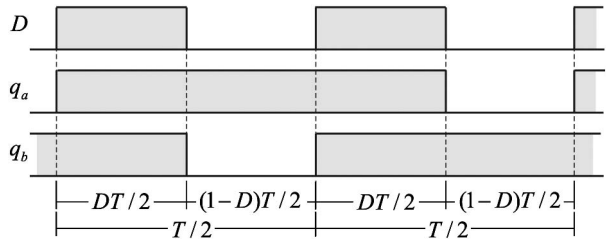

Fig. 3. Typical duty cycle D and gating signals for power switches q_a and q_b.

$$E = \frac{n}{1-D}V. \tag{2}$$

When designing a push–pull converter, it is convenient to select the transformer turns ratio n such that duty cycle D does not vary in a wide range. At the same time, high values for n should be avoided to ensure that the pulsewidth modulation (PWM) voltage inverter operates with low modulation index.

A. Push–Pull Gain

Acting as an adjustable-ratio dc transformer, the dc/dc converter allows impedance matching between the panels and the motor that drives the centrifugal pump. The choice of converter gain is most easily explained using an example. Consider the following: 1) The electrical load is a 220 V/60 Hz 1.5 hp induction motor; 2) the photovoltaic array is composed of ten 130 Wp panels arranged in a 2 (series) × 5 (parallel) layout; and 3) the losses are neglected. Fig. 4 shows the mechanical torque of the motor, the pump characteristic (upper plot), and the motor efficiency (lower plot) curves as functions of rotor (mechanical) speed. Assuming that the motor operates at a constant volt/hertz ratio, the operating points are determined by the intersection of the mechanical torque and load (pump) characteristic curves. Based on the power level demanded by the load, it is possible to determine the numerical values for the input and output push–pull voltages. For each operating point, therefore, it is possible to recover values for the motor line voltage to determine the minimum required dc-bus voltage, which corresponds to the push–pull output voltage. The push–pull input voltage is the MPPT panel array voltage. Thus, given the motor output power, it is possible to numerically find the push–pull input voltage.

The design of the minimum push–pull gain [i.e., the high-frequency voltage transformer ratio (n)] can be found in two different ways. On the one hand, it is possible to consider that a

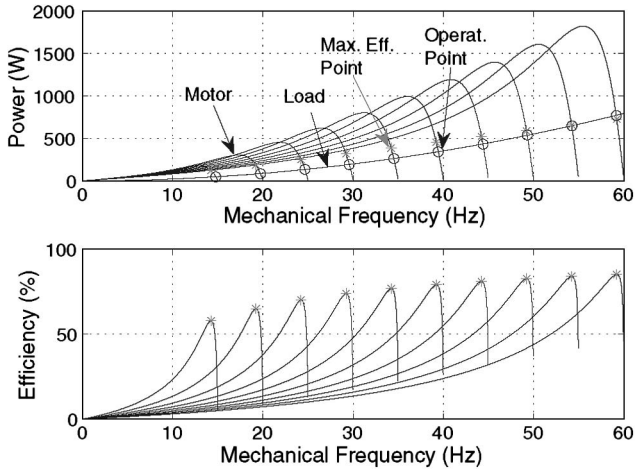

Fig. 4. (Top) Power profiles of mechanical motor output and load as a function of mechanical frequency. (Bottom) Motor efficiency as a function of mechanical frequency.

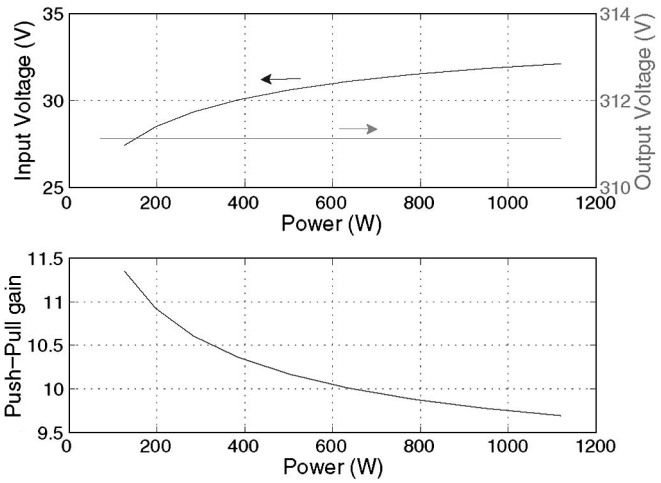

Fig. 5. (Top) Input and output voltages for a stiff dc-bus voltage and (bottom) push–pull gain.

stiff dc-bus is desired and that motor voltage is regulated by the inverter modulation index depending on the available power. On the other hand, it is possible to keep the inverter modulation index at a maximum value, leaving the output voltage to vary freely with the available power. In Figs. 5 and 6, the input and output voltages (upper plot) and the push–pull gain (lower plot) are shown as functions of the available power. In Fig. 5, a stiff dc-bus is adopted, while in Fig. 6, the dc-bus voltage varies with the available power.

In order to select the minimum push–pull gain, it is necessary to take into account the fact that the maximum efficiency of a push–pull converter is reached when $D \to 0$. It is also important to be aware that push–pull efficiency decreases when operating in a lower than rated power range. Finally, if the motor operates with a low modulation index ($\ll 1$), the total harmonic distortion and motor losses increase. Here, n was selected by assuming that when the push–pull converter runs below half rated power, D must be zero. From Fig. 6 (bottom), $n = 6.5$ is a reasonable tradeoff for the conflicting design objectives.

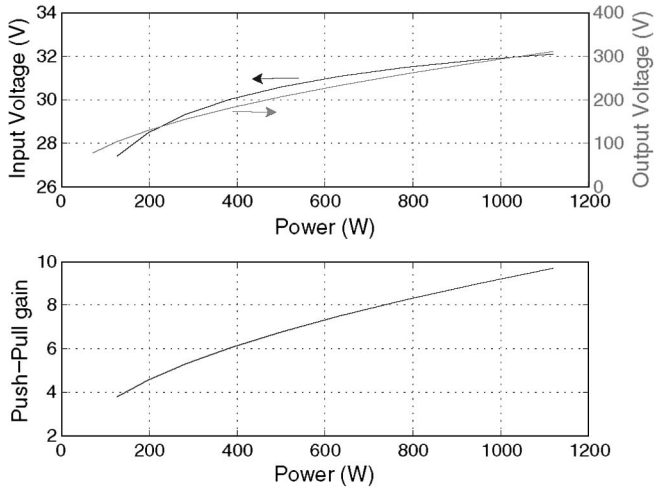

Fig. 6. (Top) Input and output voltages for a variable dc-bus voltage and (bottom) push–pull gain.

III. Induction Motor

The three-phase induction motor is still very attractive for a wide range of applications due to its robust construction and low cost. However, to use this type of motor for photovoltaic pumping, we must consider the following basic requirements: 1) control based on power availability and 2) efficiency maximization. In the analysis here, we will use the following dynamic model of a three-phase motor:

$$v^a_{sdq} = r_s i^a_{sdq} + \frac{d\lambda^a_{sdq}}{dt} + j\omega_a \lambda^a_{sdq} \tag{3}$$

$$0 = r_r i^a_{rdq} + \frac{d\lambda^a_{rdq}}{dt} + j(\omega_a - \omega_r)\lambda^a_{rdq} \tag{4}$$

$$\lambda^a_{sdq} = l_s i^a_{sdq} + l_m i^a_{rdq} \tag{5}$$

$$\lambda^a_{rdq} = l_r i^a_{rdq} + l_m i^a_{sdq} \tag{6}$$

$$T_e = P\frac{l_m}{l_r}\left(i^a_{sq}\lambda^a_{rd} - i^a_{sd}\lambda^a_{rq}\right) \tag{7}$$

$$\frac{d\omega_r}{dt} = \frac{P}{J_m}(T_e - T_m) - \frac{F_m}{J_m}\omega_r \tag{8}$$

where the index a denotes that the electrical variables are expressed in terms of an arbitrary reference frame. The variables and parameters used in the aforementioned expressions are defined as follows: 1) $v^a_{sdq} = v^a_{sd} + jv^a_{sq}$, $i^a_{sdq} = i^a_{sd} + ji^a_{sq}$, $i^a_{rdq} = i^a_{rd} + ji^a_{rq}$, $\lambda^a_{sdq} = \lambda^a_{sd} + j\lambda^a_{sq}$, and $\lambda^a_{rdq} = \lambda^a_{rd} + j\lambda^a_{rq}$ denote the stator voltage, the stator current, the rotor current, the stator flux, and the rotor flux vectors, respectively; 2) ω_r, ω_a, T_e, and T_m represent the angular shaft speed, the angular speed of the dq coordinate system, the electromagnetic torque, and the load torque, respectively; and 3) P, J_m, F_m, r_s, r_r, l_s, l_r, and l_m are the number of pole pairs, the moment of inertia, the viscous friction coefficient, the stator resistance, the rotor resistance, the self-inductance of the stator, the self-inductance of the rotor, and the mutual inductance between the stator and rotor, respectively.

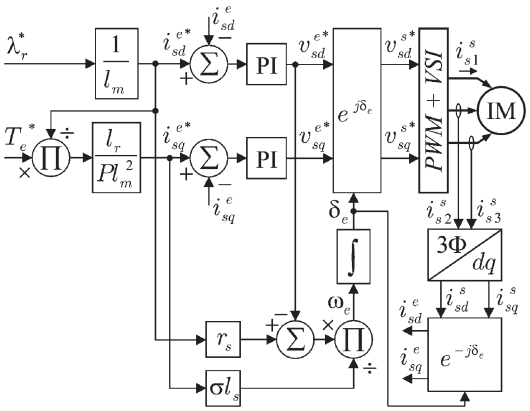

Fig. 7. Induction motor control system: Combining the IFOC strategy with a virtual speed sensor based on the d-axis voltage equation.

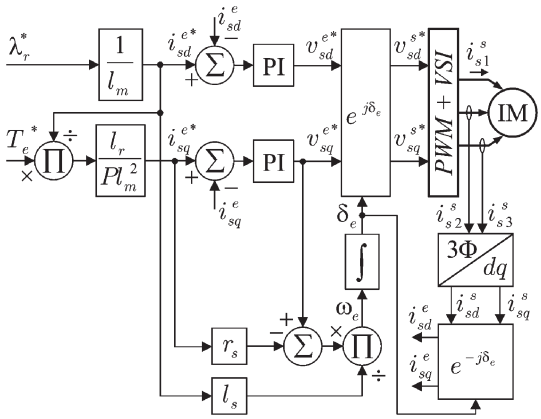

Fig. 8. Induction motor control system: Combining the IFOC strategy with a virtual speed sensor based on the q-axis voltage equation.

A. Motor Control

High-performance induction motor control can be realized using field-oriented control strategies. In photovoltaic pumping, motor control must be focused on maximizing the power delivered and motor efficiency. Power delivery maximization can be realized through torque control, while motor efficiency can be optimized by controlling the motor magnetic flux level. Fig. 4 shows that the induction motor runs at low efficiency when electrical frequency is reduced. This occurs because, at low speed, the motor runs at almost no load. By adjusting the magnetic flux level, one may move the motor operating point toward that of maximum efficiency.

Obviating the requirement for a physical speed sensor is one of the main ways of increasing the robustness of the system. Three different sensorless techniques have been evaluated. Two of these techniques are derived from the indirect field-oriented control (IFOC) scheme, and the third one is the well-known direct torque control (DTC) technique. In all cases, the power delivery is determined by the electromagnetic torque reference.

Fig. 7 shows the block diagram of an induction motor control system in which the IFOC strategy is combined with a virtual speed sensor based on the d-axis voltage equation. In this case, the speed estimate is determined from the d-axis stator voltage equation written for a reference frame aligned with the rotor flux $(a = e)$. The rotor flux angular frequency can be computed from

$$\omega_e = \frac{-\left(v_{sd}^{e*} - r_s i_{sd}^{e*}\right)}{\sigma l_s i_{sq}^{e*}}. \tag{9}$$

Fig. 8 shows the block diagram of an induction motor control system in which the IFOC strategy is combined with a virtual speed sensor based on the q-axis voltage equation. In this case, the speed estimate is determined from the q-axis stator voltage equation written for a reference frame aligned with the rotor flux $(a = e)$. The rotor flux angular frequency is then computed from

$$\omega_e = \frac{v_{sq}^{e*} - r_s i_{sq}^{e*}}{l_s i_{sd}^{e*}}. \tag{10}$$

Fig. 9 shows the block diagram of an induction motor control system where the DTC strategy is combined with a virtual sensor that provides electromagnetic torque and magnetic flux estimates. The convergence time of all three control strategies (Figs. 7–9) has been evaluated by numerical simulation. The results are summarized in Table I.

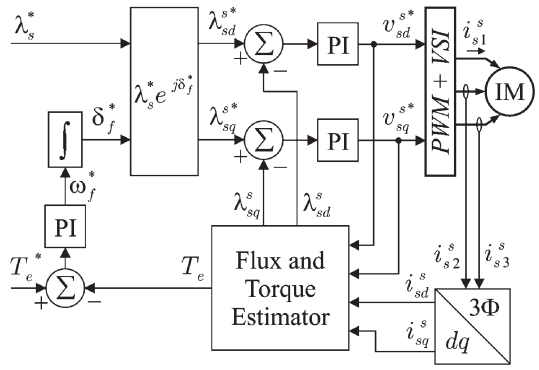

Fig. 9. Block diagram of an induction motor control system: Combining the DTC strategy with a virtual sensor providing electromagnetic torque and magnetic flux estimates.

TABLE I
CONVERGENCE TIME OF INDUCTION MOTOR CONTROL STRATEGIES FOR STEP CHANGE IN REFERENCE TORQUE

IFOC		DTC
d-axis	q-axis	
0.4s	0.8s	0.7s

To establish an efficient power flow from the panels to the motor, the dc-bus voltage plays an important role. From the push–pull gain

$$\frac{E}{V} = \frac{n}{1 - D} \tag{11}$$

it can be seen that the dc-bus reference voltage (E^*) depends on the actual input voltage and the reference duty cycle value

$$E^* = \frac{n}{1 - D^*} V \tag{12}$$

thus ensuring that the photovoltaic array delivers maximum available power. Power flow can therefore be set using the dc-bus voltage control. It is important to note that $\min(E^*) \approx nV$. From here on, the reference motor torque (T_e^*) will be

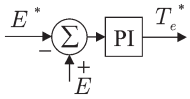

Fig. 10. Regulating the dc-bus voltage by adjusting the electromagnetic torque of the induction motor.

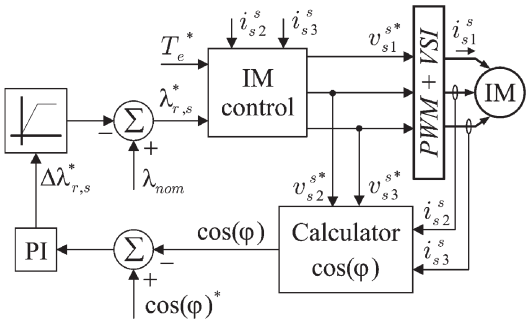

Fig. 11. Block diagram of a motor control system where a feedback loop for adjusting the power factor has been added.

generated from the dc-bus voltage error $(E - E^*)$, as shown by the feedback control loop in Fig. 10. The maximization of induction motor efficiency is discussed in the next section.

B. Motor Optimization

The basic motivation for motor efficiency improvement is to save energy. For a given motor, the objective is to deliver a given mechanical (output) power with a minimum of electrical (input) power. The usual approach when seeking efficiency improvement is to assume that the motor is in steady state, i.e., running at constant speed. In photovoltaic pumping, this assumption cannot be made.

Induction motors are designed to exhibit high efficiency when operating at rated load and fed with rated voltage at rated frequency. Nevertheless, induction motors can be used in variable-speed variable-load applications. It is necessary in such applications, however, to adjust either the voltage, the frequency, or both. In these cases, high-efficiency operation is still possible by selecting an appropriate value for the magnetic flux level of the motor. In the work reported here, three different methods for selecting the magnetic flux level are evaluated. The methods are based on power factor adjustment, empirical search for a minimum-loss operating point, and balanced d and q currents. The use of either rotor or stator magnetic flux for motor efficiency improvement is a direct consequence of the control strategy chosen in the previous sections.

1) Power Factor: Induction motors are designed to exhibit high power factor when operating at rated load. Deviation from rated conditions requires power factor adjustment, which can be implemented by changing the magnetic excitation of the motor. Fig. 11 shows a block diagram of a motor control system that includes a feedback loop for adjusting the power factor. In this block diagram, the power factor $[\cos(\varphi)]$ is calculated by using the reference stator voltages (v^*_{s2}, v^*_{s3}) and the measured stator currents (i^*_{s2}, i^*_{s3}). The power factor error $[\cos(\varphi^*) - \cos(\varphi)]$ is processed by a proportional–integral (PI) controller to adjust the magnetic flux $(\lambda^*_{r,s})$. The tuning of this PI controller is a

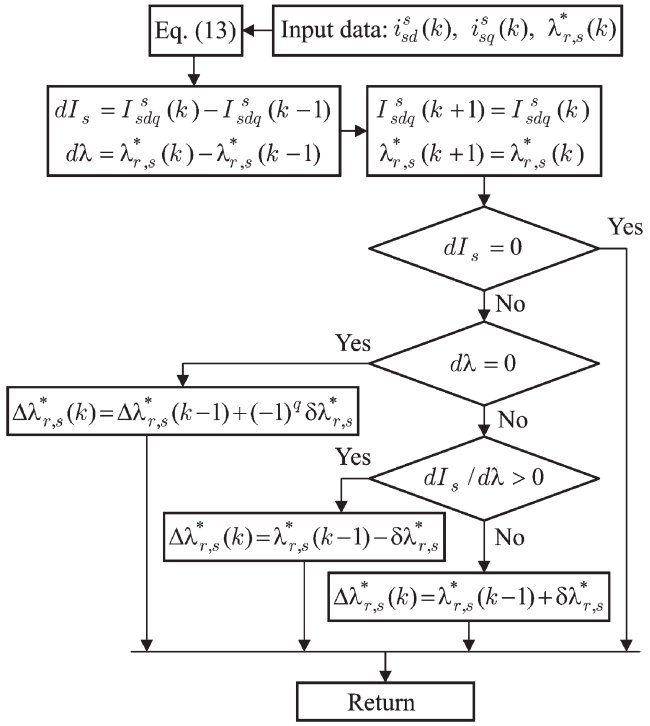

Fig. 12. P&O algorithm flowchart: Optimizing the magnetic flux level for a given stator current.

relatively complex task since there is no explicit model for the system to be controlled. As a guideline, a relatively slow closed-loop system should be designed. The use of stator, or rotor, flux as a control variable depends on what motor control strategy is chosen. The "IM control" block denotes one of the three control strategies previously discussed (see Figs. 7–9).

2) Empirical Search: This optimization method is based on a trial-and-error procedure. The output torque is kept at a constant value, and the control variable (rotor or stator flux) is adjusted to minimize the input power [33]. An alternative implementation in which the stator current

$$I^s_{sdq} = \sqrt{\left(i^s_{sd}\right)^2 + \left(i^s_{sq}\right)^2} \tag{13}$$

is minimized instead of the input power can also be used [40]. The perturb-and-observe (P&O) optimization algorithm is adopted to establish the new reference value for the control variable $(\lambda^*_{r,s})$ for a given stator current measurement. Fig. 12 shows the basic flowchart of the P&O algorithm. It is worth noting that exponent "q" is a random variable generated to start a new P&O cycle when the motor operates at an apparently optimal operating point. Fig. 13 shows the block diagram of an induction motor control system in which this empirical search algorithm is combined with the IFOC strategy.

3) Current Balance: This method is based on stator current amplitude control seen from the rotor flux reference frame and can be explained as follows. From (7), one can compute the electromagnetic torque as a function of stator current, i.e.,

$$T_e = \frac{Pl^2_m}{l_r} i^e_{sd} i^e_{sq}. \tag{14}$$

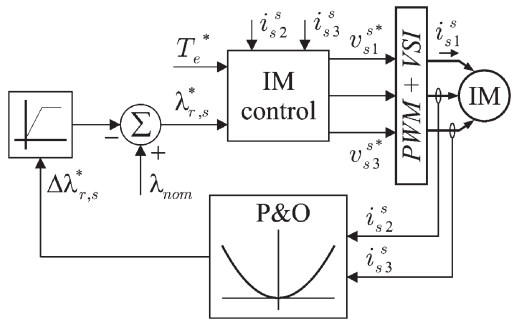

Fig. 13. Induction motor control system based on the IFOC strategy combined with an empirical search method to optimize the magnetic flux level.

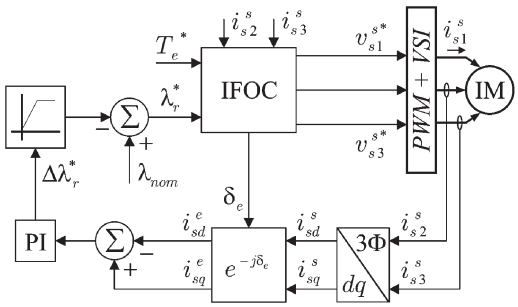

Fig. 14. Induction motor control system based on the IFOC strategy combined with the balancing current method to optimize the magnetic flux level.

Assuming constant stator current I_{sdq} and eliminating i_{sd}^e from (14) yield

$$T_e = \frac{Pl_m^2}{l_r} i_{sq}^e \sqrt{(I_{sdq})^2 - \left(i_{sq}^e\right)^2}.$$

Based on this equation, the maximum torque will be observed when

$$\frac{dT_e}{di_{sq}^e} = 0. \tag{15}$$

After solving (15), $(I_{sdq})^2$ is replaced by $(i_{sd}^e)^2 + (i_{sq}^e)^2$, which leads to the conclusion that maximum torque occurs when $i_{sd}^e = i_{sq}^e$. Fig. 14 shows the block diagram of an induction motor control system in which the current-balancing algorithm is combined with the IFOC strategy. The current-balancing error is processed by a PI controller for adjusting the magnetic flux (λ_r^*).

IV. Control and Optimization Procedure Evaluation

The previous discussion was intended to show viable options for an effective energy processing strategy for a photovoltaic pumping system. In simulations, all the control strategies presented the same overall performance. Experimental test results, however, showed that, despite not depending on electrical rotor parameters, the DTC solution (Fig. 9) is not stable during start-up. The same is true for IFOC combined with the d-axis voltage model (Fig. 7), in which a low reference torque value results in a small denominator. The experimental evaluation presented here has therefore been restricted to IFOC combined with the q-axis voltage model (Fig. 8).

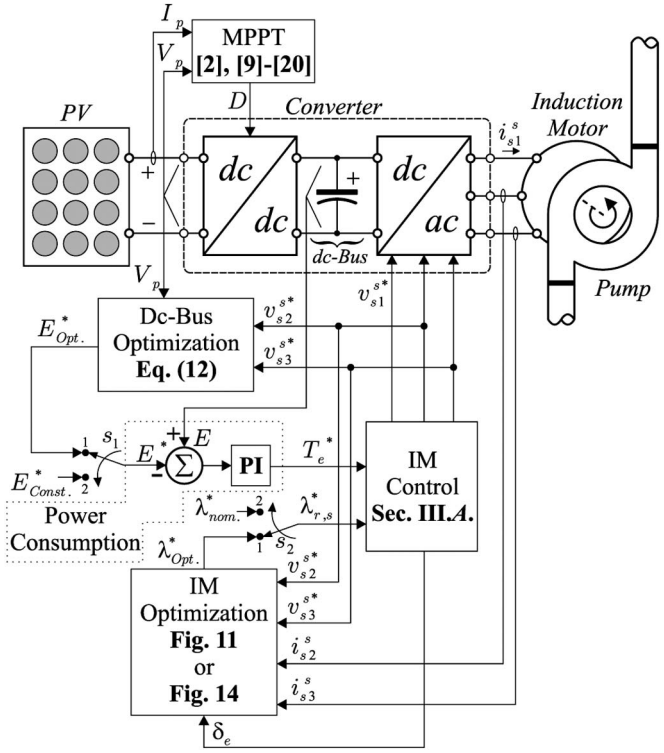

Fig. 15. Experimental photovoltaic pumping test platform in which all the optimization loops have been implemented.

The experimental setup comprises ten 130 Wp panels arranged in a 2 (series) × 5 (parallel) layout, a 1 kW push–pull converter (transformer turns ratio $n = 6$), a 1.5 hp 220 V/60 Hz three-phase induction motor, and a 1.5 hp centrifugal pump. The hydraulic circuit is a closed loop with admission and output valves that allow the rated load to be defined. The overall system control runs on a TMS320F2812 processor, which is responsible for controlling the power flow, including the push–pull converter and the three-phase voltage-source inverter.

Fig. 15 shows the block diagram of the experimental photovoltaic pumping test system in which all the optimization procedures have been implemented. In this test system, the dc/dc converter is responsible for tracking the MPP of the photovoltaic array, whereas the dc/ac converter is responsible for controlling the induction motor.

To understand the optimization process, it is important to realize that the dc-bus voltage is a common variable for both converters. Depending on how the dc-link reference voltage is computed, it is possible to obtain two different levels of optimization. In one case, the dc-link reference voltage is determined from the rated motor voltage $(E_{Const.}^*)$. Since insolation varies slowly (compared with optimization algorithm convergence time), optimization of motor efficiency can be performed assuming that torque and motor speed are constant. This can be interpreted as a conventional optimization procedure in which a stiff dc-link voltage is available. This implies that the PWM waveform applied to the motor by the voltage inverter will have high modulation index in a wide power range. In the second case, optimization is obtained by forcing the duty cycle D to be

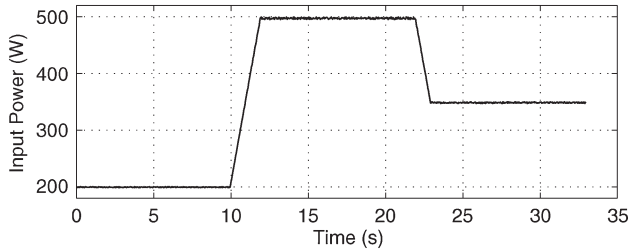

Fig. 16. Profile of the input power supplied to the push–pull converter—controlled dc source test.

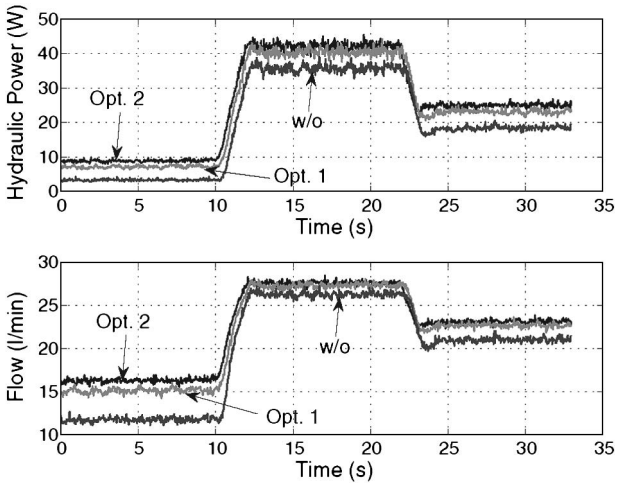

Fig. 17. (Top) Hydraulic power and (bottom) pump flow measured at the pump outlet when the system operates without optimization and with the following two levels of optimization: 1) (Opt. 1) Motor optimization $[\cos(\varphi)]$ only and 2) (Opt. 2) push–pull converter optimization plus induction motor optimization.

minimal, resulting in a minimum output voltage of the dc/dc converter and thus reducing switching power losses in both converters. Then, the dc-link voltage $(E^*_{Opt.})$ can be determined either from the reference output voltage (v^*_{s2} and v^*_{s3}) or from the push–pull input voltage (nV_p).

The optimization method shown in Fig. 13 does not work due to the stochastic nature of the input power.

Initially, the photovoltaic array was replaced by a controlled dc voltage source to ensure fair comparison between tests. The push–pull converter controls the input current in such a way that, over a period of 33 s, the input power attains three different levels, i.e., 200, 500, and 350 W. To move from one power level to another, we choose a power rate of change that is compatible with a realistic profile of insolation variation. This is important since sensorless control is sensitive to abrupt changes. Fig. 16 shows the profile of the input power supplied to the push–pull converter.

From the experimental results, we can verify the effectiveness of the proposed optimization procedures by comparing the system performance without any optimization and with the following two optimization levels: 1) only induction motor optimization, i.e., Opt. 1, and 2) push–pull converter and induction motor optimization, i.e., Opt. 2. Fig. 17 shows the hydraulic power and the pump flow with and without optimization of the power factor. We clearly see how the power conversion is more effective when optimization procedures are included. Note that

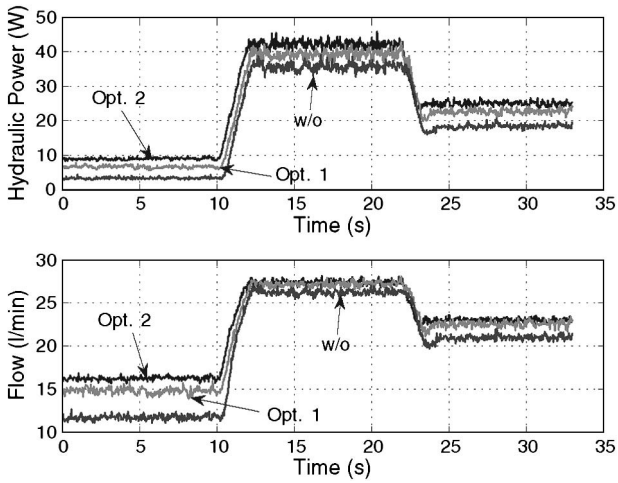

Fig. 18. (Top) Hydraulic power and (bottom) pump flow measured at the pump outlet without optimization and with the following two levels of optimization: 1) (Opt. 1) Induction motor optimization (balanced stator currents) only and 2) (Opt. 2) push–pull converter optimization plus induction motor optimization.

TABLE II
SYSTEM ENERGY BALANCE REGARDING FIGS. 16–18

	w/o Opt.	Optimized			
		Power Factor		Balanced Current	
	$\lambda^*_r = 0.826$	Opt. 1	Opt. 2	Opt. 1	Opt. 2
Volume pumped (liters)	10.06	11.56	12.14	11.30	11.91
Hydraulic energy (J)	510.84	700.78	833.09	664.46	784.00
Input energy (kJ)	11.59	11.58	11.57	11.57	11.59
Efficiency %	4.41	6.05	7.20	5.74	6.76

allowing dc-bus voltage reduction helps improve the hydraulic power. When comparing the results shown in Fig. 17, it is important to consider that Opt. 1 means only induction motor optimization, while Opt. 2 means that the push–pull converter is also optimized.

A second set of results (Fig. 18) illustrates how the balanced stator current technique positively affects pumping system efficiency, showing a visible augmentation of both power delivered and pump flow when the system is optimized. At low input power levels, the relative gain increases. Table II summarizes the data from the experimental tests. This table shows the percentage augmentation of the pumped volume and the energy with respect to the nonoptimized condition. From Table II, it can be seen that system efficiency increases by 63% when both induction motor and dc-link voltage are optimized (Opt. 2).

In this last test, the controlled dc voltage source was replaced by the photovoltaic panel array, allowing evaluation of the pumping under realistic conditions. Again, IFOC combined with the q-axis voltage model solution (Fig. 8) exhibited greater stability over the entire operating range. All experimental results obtained in this test were therefore obtained with this control strategy. From the results shown in Figs. 19–21, it is possible to verify the power flow at different points of the system and the variation of their profiles with sun radiation (see Table III). It is interesting to note that the efficiency in these tests is higher than that in the previous tests (see Table II). This is expected because the efficiency is higher when the system runs at rated power. The efficiency improvement, however, is more perceptible when the system runs at low power.

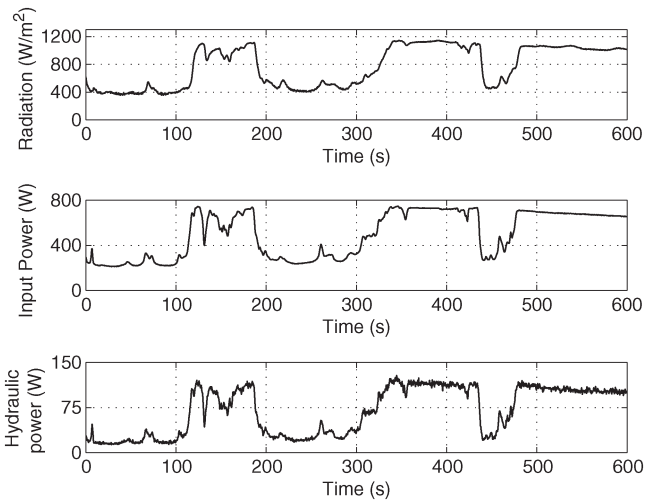

Fig. 19. Measured power when the system operates without any optimization procedure. (From top to bottom) Sun radiation profile, power delivered from the photovoltaic array, and hydraulic power.

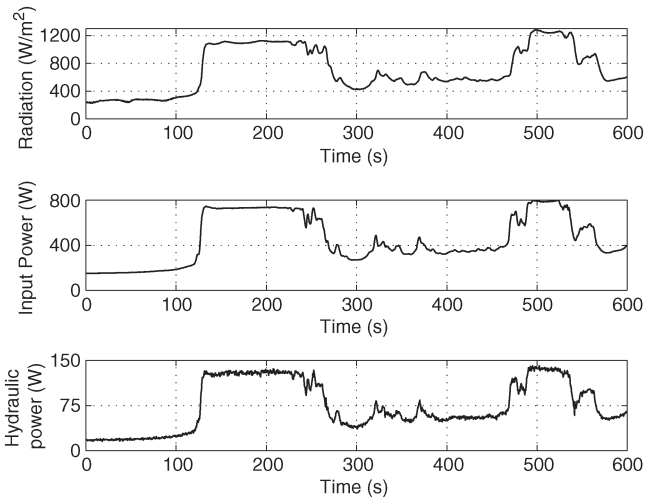

Fig. 20. Measured power when the system operates with the push–pull and motor optimization $[\cos(\varphi)]$ procedure. (From top to bottom) Sun radiation profile, power delivered from the photovoltaic array, and hydraulic power.

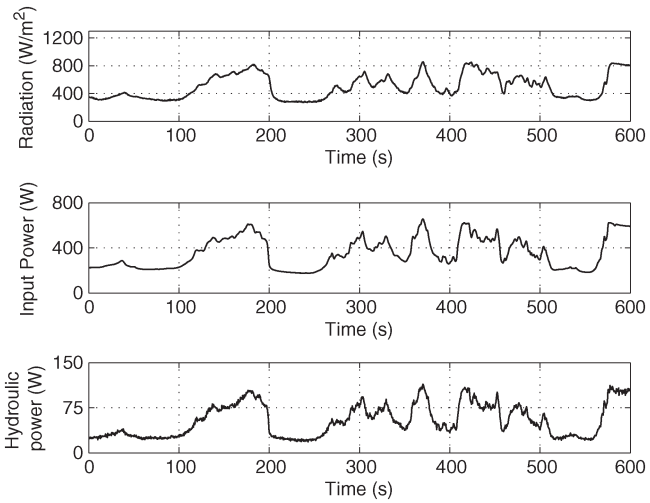

Fig. 21. Measured power when the system operates with the push–pull and motor optimization (balanced currents) procedure. (From top to bottom) Sun radiation profile, power delivered from the photovoltaic array, and hydraulic power.

TABLE III
SYSTEM ENERGY BALANCE REGARDING FIGS. 19–21

	w/o Opt.	Optimized	
		Power Factor	Balanced Current
	$\lambda_r^* = 0.826$	Opt. 2	Opt. 2
Volume pumped (liters)	221.63	205.97	190.70
Hydraulic energy (kJ)	48.30	44.60	32.20
Input energy (kJ)	338.00	270.00	212.00
Efficiency %	14.30	16.51	15.16

V. CONCLUSION

This paper has evaluated several control strategies and optimization procedures that can be used for implementing an effective photovoltaic pumping system. The principal contributions are related to the design of the step-up converter and to the optimization of the induction motor efficiency. With respect to converter design, we have shown that when the dc-bus varies with available power, it is possible to improve its efficiency. In terms of induction motor control, among the three sensorless alternatives evaluated, IFOC combined with the q-axis voltage model was the most stable at start-up. On the other hand, power factor optimization was the best solution in terms of pumping system efficiency. When using balanced current, it is not necessary to set any reference value. This results in a simpler scheme than power factor adjustment (which needs a reference value that is not easy to compute over the whole operating range). It was not possible to apply a search algorithm successfully due to the stochastic nature of sunlight.

REFERENCES

[1] R. Gules, J. D. P. Pacheco, H. L. Hey, and J. Imhoff, "A maximum power point tracking system with parallel connection for PV stand-alone applications," *IEEE Trans. Ind. Electron.*, vol. 55, no. 7, pp. 2674–2683, Jul. 2008.

[2] N. Femia, G. Lisi, G. Petrone, G. Spagnuolo, and M. Vitelli, "Distributed maximum power point tracking of photovoltaic arrays: Novel approach and system analysis," *IEEE Trans. Ind. Electron.*, vol. 55, no. 7, pp. 2610–2621, Jul. 2008.

[3] D. Holmes, P. Atmur, C. Beckett, M. Bull, W. Kong, W. Luo, D. Ng, N. Sachchithananthan, P. Su, D. Ware, and P. Wrzos, "An innovative, efficient current-fed push–pull grid connectable inverter for distributed generation systems," in *Proc. IEEE PESC*, 2006, pp. 1–7.

[4] Y. Chen and K. Smedley, "A cost-effective single-stage inverter with maximum power point tracking," *IEEE Trans. Power Electron.*, vol. 19, no. 5, pp. 1289–1294, Sep. 2004.

[5] S. Busquets-Monge, J. Rocabert, P. Rodriguez, S. Alepuz, and J. Bordonau, "Multilevel diode-clamped converter for photovoltaic generators with independent voltage control of each solar array," *IEEE Trans. Ind. Electron.*, vol. 55, no. 7, pp. 2713–2723, Jul. 2008.

[6] J.-M. Kwon, B.-H. Kwon, and K.-H. Nam, "Three-phase photovoltaic system with three-level boosting MPPT control," *IEEE Trans. Ind. Electron.*, vol. 23, no. 5, pp. 2319–2327, Sep. 2008.

[7] K. K. Tse, B. M. T. Ho, H. S. H. Chung, and S. Y. R. Hui, "A comparative study of maximum-power-point trackers for photovoltaic panels using switching-frequency modulation scheme," *IEEE Trans. Ind. Electron.*, vol. 51, no. 2, pp. 410–418, Apr. 2004.

[8] W. Xiao, N. Ozog, and W. G. Dunford, "Topology study of photovoltaic interface for maximum power point tracking," *IEEE Trans. Ind. Electron.*, vol. 54, no. 3, pp. 1696–1704, Jun. 2007.

[9] N. Femia, G. Petrone, G. Spagnuolo, and M. Vitelli, "Optimization of perturb and observe maximum power point tracking method," *IEEE Trans. Power Electron.*, vol. 20, no. 4, pp. 963–973, Jul. 2005.

[10] W. Xiao, M. G. J. Lind, W. G. Dunford, and A. Capel, "Real-time identification of optimal operating points in photovoltaic power systems," *IEEE Trans. Ind. Electron.*, vol. 53, no. 4, pp. 1017–1026, Jun. 2006.

[11] J.-H. Park, J.-Y. Ahn, B.-H. Cho, and G.-J. Yu, "Dual-module-based maximum power point tracking control of photovoltaic systems," *IEEE Trans. Ind. Electron.*, vol. 53, no. 4, pp. 1036–1047, Jun. 2006.

[12] T. Esram, J. W. Kimball, P. T. Krein, P. L. Chapman, and P. Midya, "Dynamic maximum power point tracking of photovoltaic arrays using ripple correlation control," *IEEE Trans. Power Electron.*, vol. 21, no. 5, pp. 1282–1291, Sep. 2006.

[13] M. Vitorino, L. Hartmann, A. Lima, and M. Correa, "Using the model of the solar cell for determining the maximum power point of photovoltaic systems," in *Proc. EPE*, 2007, pp. 1–10.
[14] T. Esram and P. L. Chapman, "Comparison of photovoltaic array maximum power point tracking techniques," *IEEE Trans. Energy Convers.*, vol. 22, no. 2, pp. 439–449, Jun. 2007.
[15] C. Rodriguez and G. A. J. Amaratunga, "Analytic solution to the photovoltaic maximum power point problem," *IEEE Trans. Circuits Syst. I, Reg. Papers*, vol. 54, no. 9, pp. 2054–2060, Sep. 2007.
[16] W. Xiao, W. G. Dunford, P. R. Palmer, and A. Capel, "Application of centered differentiation and steepest descent to maximum power point tracking," *IEEE Trans. Ind. Electron.*, vol. 54, no. 5, pp. 2539–2549, Oct. 2007.
[17] J. W. Kimball and P. T. Krein, "Discrete-time ripple correlation control for maximum power point tracking," *IEEE Trans. Power Electron.*, vol. 23, no. 5, pp. 2353–2362, Sep. 2008.
[18] F. Liu, S. Duan, F. Liu, B. Liu, and Y. Kang, "A variable step size INC MPPT method for PV systems," *IEEE Trans. Ind. Electron.*, vol. 55, no. 7, pp. 2622–2628, Jul. 2008.
[19] M. Fortunato, A. Giustiniani, G. Petrone, G. Spagnuolo, and M. Vitelli, "Maximum power point tracking in a one-cycle-controlled single-stage photovoltaic inverter," *IEEE Trans. Ind. Electron.*, vol. 55, no. 7, pp. 2684–2693, Jul. 2008.
[20] V. V. R. Scarpa, S. Buso, and G. Spiazzi, "Low-complexity MPPT technique exploiting the PV module MPP locus characterization," *IEEE Trans. Ind. Electron.*, vol. 56, no. 5, pp. 1531–1538, May 2009.
[21] H. Patel and V. Agarwal, "Maximum power point tracking scheme for PV systems operating under partially shaded conditions," *IEEE Trans. Ind. Electron.*, vol. 55, no. 4, pp. 1689–1698, Apr. 2008.
[22] L. Gao, R. A. Dougal, S. Liu, and A. P. Iotova, "Parallel-connected solar PV system to address partial and rapidly fluctuating shadow conditions," *IEEE Trans. Ind. Electron.*, vol. 56, no. 5, pp. 1548–1556, May 2009.
[23] G. Carannante, C. Fraddanno, M. Pagano, and L. Piegari, "Experimental performance of MPPT algorithm for photovoltaic sources subject to inhomogeneous insolation," *IEEE Trans. Ind. Electron.*, vol. 56, no. 11, pp. 4374–4380, Nov. 2009.
[24] D. Sera, R. Teodorescu, J. Hantschel, and M. Knoll, "Optimized maximum power point tracker for fast changing environmental conditions," in *Proc. IEEE ISIE*, 2008, pp. 2401–2407.
[25] E. Muljadi, "PV water pumping with a peak-power tracker using a simple six-step square-wave inverter," *IEEE Trans. Ind. Appl.*, vol. 33, no. 3, pp. 714–721, May/Jun. 1997.
[26] G. Heng, X. Zheng, L. You-Chun, and W. Hui, "A novel maximum power point tracking strategy for stand-alone solar pumping systems," in *Proc. IEEE/PES Conf. Exhib. Transmiss. Distrib.*, 2005, pp. 1–5.
[27] V. Vongmanee, "The vector control inverter for a PV motor drive system implemented by a single chip DSP controller ADMC331," in *Proc. IEEE APCCAS*, 2002, pp. 447–451.
[28] A. Betka and A. Moussi, "Performance optimization of a photovoltaic induction motor pumping system," *Renewable Energy*, vol. 29, no. 14, pp. 2167–2181, Nov. 2004.
[29] M. Mimouni, M. Mansouri, B. Benghanem, and M. Annabi, "Vectorial command of an asynchronous motor fed by a photovoltaic generator," *Renewable Energy*, vol. 29, no. 3, pp. 433–442, Mar. 2004.
[30] M. Arrouf and N. Bouguechal, "Vector control of an induction motor fed by a photovoltaic generator," *Appl. Energy*, vol. 74, no. 1/2, pp. 159–167, Jan./Feb. 2003.
[31] J. Arribas and C. González, "Optimal vector control of pumping and ventilation induction motor drives," *IEEE Trans. Ind. Electron.*, vol. 49, no. 4, pp. 889–895, Aug. 2002.
[32] B. Singh, B. Singh, B. Singh, A. Chandra, and K. Al-Haddad, "Optimized performance of solar-powered variable speed induction motor drive," in *Proc. IEEE PEDES*, 1996, pp. 58–66.
[33] D. Kirschen, D. Novotny, and T. Lipo, "On-line efficiency optimization of a variable frequency induction motor drive," *IEEE Trans. Ind. Appl.*, vol. IA-21, no. 3, pp. 610–616, May/Jun. 1985.
[34] F. Abrahamsen, F. Blaabjerg, J. Pedersen, P. Grabowski, and P. Thogersen, "On the energy optimized control of standard and high-efficiency induction motors in CT and HVAC applications," *IEEE Trans. Ind. Appl.*, vol. 34, no. 4, pp. 822–831, Jul./Aug. 1998.
[35] F. Abrahamsen, F. Blaabjerg, J. K. Pedersen, and P. Thggersen, "Efficiency optimized control of medium-size induction motor drives," in *Conf. Rec. IEEE-IAS Annu. Meeting*, 2000, pp. 1489–1496.
[36] F. Abrahamsen, "Energy optimal control of induction motor drives," Ph.D. thesis, Aalborg University, Denmark, Feb. 2000.
[37] C. C. de Azevedo, C. B. Jacobina, L. A. S. Ribeiro, A. M. N. Lima, and A. C. Oliveira, "Indirect field orientation for induction motors without speed sensor," in *Proc. IEEE APEC*, 2002, pp. 809–814.
[38] M. B. R. Corrêa, C. B. Jacobina, P. M. dos Santos, E. C. dos Santos, and A. M. N. Lima, "Sensorless control strategies for single-phase induction motor drive system," in *Proc. IEEE PESC*, 2005, pp. 707–713.
[39] M. A. Vitorino, M. B. R. Correa, C. B. Jacobina, and A. M. N. Lima, "Sensorless induction motor drive for photovoltaic pumping applications," in *Proc. IEEE APEC*, Feb. 2008, pp. 1139–1143.
[40] I. Kioskeridis and N. Margaris, "Loss minimization in scalar-controlled induction motor drives with search controllers," *IEEE Trans. Power Electron.*, vol. 11, no. 2, pp. 213–220, Mar. 1996.

Montiê Alves Vitorino was born in Campina Grande, Brazil, in 1983. He received the B.S. and M.S. degrees in electrical engineering from the Federal University of Campina Grande, Campina Grande, in 2007 and 2008, respectively, where he is currently working toward the Ph.D. degree in the Department of Electrical Engineering.

Maurício Beltrão de Rossiter Corrêa (S'97–M'03) was born in Maceió, Brazil, in 1973. He received the B.S., M.S., and Ph.D. degrees in electrical engineering from the Federal University of Paraíba, Campina Grande, Brazil, in 1996, 1997, and 2002, respectively.

From 1997 to 2004, he was with the Centro Federal de Educacão Tecnológica de Alagoas, Palmeira dos Índios, Brazil. From 2001 to 2002, he was with the Wisconsin Electric Machines and Power Electronics Consortium, University of Wisconsin, Madison, as a Scholar. Since July 2004, he has been with the Department of Electrical Engineering, Federal University of Campina Grande, Campina Grande, Brazil, where he is currently an Associate Professor of electrical engineering. His research interests include electrical drives, power electronics, and renewable energy.

Cursino Brandão Jacobina (S'78–M'78–SM'98) was born in Correntes, Brazil, in 1955. He received the B.S. degree in electrical engineering from the Federal University of Paraíba, Campina Grande, Brazil, in 1978 and the Diplôme d'Études Approfondies and Ph.D. degrees from the Institut National Polytechnique de Toulouse, Toulouse, France, in 1980 and 1983, respectively.

From 1978 to 2002, he was with the Department of Electrical Engineering, Federal University of Paraába. Since April 2002, he has been with the Department of Electrical Engineering, Federal University of Campina Grande, Campina Grande, Brazil, where he is currently a Professor of electrical engineering. His research interests include electrical drives, power electronics, and energy systems.

Antonio Marcus Nogueira Lima (S'77–M'89–SM'05) was born in Recife, Brazil, in 1958. He received the B.S. and M.S. degrees in electrical engineering from the Federal University of Paraíba, Campina Grande, Brazil, in 1982 and 1985, respectively, and the Ph.D. degree from the Institut National Polytechnique de Toulouse, Toulouse, France, in 1989.

From 1977 to 1982, he was with the Escola Técnica Redentorista, Campina Grande, Brazil. From 1982 to 1983, he was a Project Engineer with SulAmérica Philips, Recife. From 1983 to 2002, he was with the Department of Electrical Engineering, Federal University of Paraába. Since April 2002, he has been with the Department of Electrical Engineering, Federal University of Campina Grande, Campina Grande, where he is currently a Professor of electrical engineering. His research interests are in the fields of electrical machines and drives, power electronics, electronic instrumentation, control systems, and system identification.